MR. ANDREW FROME STEPHENS (Orcid ID : 0000-0002-2271-750X)

DR. SHAUN DAVID GREGORY (Orcid ID : 0000-0002-5448-1917)

Article type : Main Text

Corresponding Author Email ID: research.andrew.stephens@gmail.com

IN-VITRO EVALUATION OF AN ADAPTIVE STARLING-LIKE CONTROLLER FOR DUAL ROTARY VENTRICULAR ASSIST DEVICES

Stephens, Andrew (proxy) (contact); Gregory, Shaun; Tansley, Geoff; Busch, Andrew; Salamonsen, Robert

Corresponding Author

Andrew Stephens

Monash University - Department of Mechanical and Aerospace Engineering

Lab 2, Level 3, Baker Heart and Diabetes Institute Prahran Victoria 3007

Australia

T: +614 37 034 036 F: NA

Received: January 28, 2019

Revised: May 19, 2019

This article has been accepted for publication and undergone full peer review but has not been through the copyediting, typesetting, pagination and proofreading process, which may lead to differences between this version and the Version of Record. Please cite this article as doi: 10.1111/aor.13510

Introduction

The Starling mechanism describes the non-linear relationship between ventricular preload and ventricular stroke work (1) and was explored by Guyton who defined an equivalent intrinsic and extrinsic response of the heart. The intrinsic response describes the non-linear relationship between ventricular preload and cardiac output through the establishment of cardiac response curves (CRC) and venous return lines (Figure 1 – solid lines) (2). The extrinsic response of the heart describes how preload sensitivity and the maximum cardiac output of the heart can increase or decrease in response to sympathetic or parasympathetic stimulation under different circulatory conditions (Figure 1 – dotted and dashed lines) (2,3). In the healthy human, the Starling mechanism determines the output of the ventricles and maintains flow balance between the pulmonary and systemic circulatory systems.

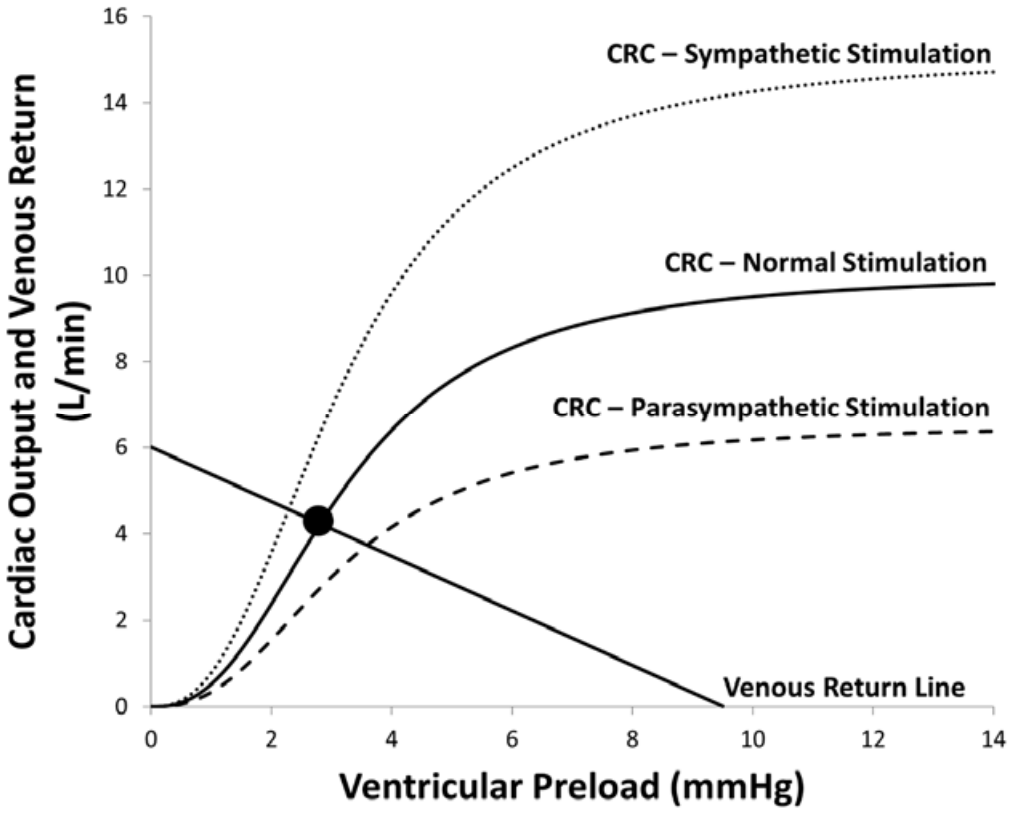

Figure 1: The Starling response is intrinsic to the heart and can be characterised by cardiac output and venous return functions (solid lines). An extrinsic response also exists which modifies the preload sensitivity of the heart (dotted lines). CRC – cardiac response curve.

In the case of heart failure, the Starling mechanism is diminished, and the heart is unable to provide adequate perfusion to meet the body's demand. Rotary ventricular assist devices (VADs) have been used to treat end-stage heart failure. However, when operated at a constant speed VADs are insufficiently sensitive to changes in preload (as a feature of their pump pressure head characteristics) when compared to the healthy heart (4,5). As a result, VADs are unable to adequately adjust their flow rate to meet the constantly changing cardiac demand from the patient. This issue is compounded in patients receiving biventricular assist device (BiVAD) support for the left and right ventricle (LV and RV) due to the lack of preload sensitivity in both VADs and the diminished Starling mechanism in both ventricles (6). Inadequate flow regulation from both VADs leaves patients vulnerable to harmful over- or under-pumping scenarios and reduced quality of life.

Physiological controllers have been designed to automatically adjust VAD speed and therefore flow to meet the varying patient cardiac demand, thereby restoring flow balance and reducing the likelihood of over- or under-pumping. Several review papers outlining and comparing different physiological controllers have demonstrated that Starling-like control (SLC) of VADs, which uses measured LV end-diastolic pressure (P_{LVED}) as a preload indicator, consistently outperforms other physiological control systems (7–11). An SLC consists of two components, a control line (CL) which emulates the native cardiac response curve, and a return path, which emulates the native venous return. When combined, the CL and return path can be used to accurately predict the required VAD flow for a given patient state. All SLCs emulate the intrinsic response of the heart. However, only a few SLCs have attempted to emulate the extrinsic response of the heart. Because both responses are extrinsic to the VAD, they are hereby referred to as the immediate (intrinsic) and adaptive (extrinsic) responses. The adaptive response plays an important role in SLC, given that in an immediate response-only SLC the VAD flow will asymptote to a fixed flow rate at very high preloads (as can be seen in Figure 1 at preloads above approximately 9 mmHg). The sigmoid nature of the CL limits the controller's ability to respond to more severe changes in the patient's condition, such as during exercise.

The development and evaluation of several SLCs have been published previously. These SLCs primarily differ in their CL shape and the type of controller return path employed. Some of the published SLCs were expanded into BiVAD-SLCs. One of the first published BiVAD-SLCs used a physiologically representative CL with a vertical return path (12). The controller included an emergency adaption mechanism which increased or decreased the CLs preload sensitivity when the operating point (OP – the combination of measured VAD flow and measured preload) moved outside a predefined control box (upper and lower limits of measured preload and VAD flow). The controller demonstrated improved preload sensitivity but unstable transient controller response, likely due to the use of a vertical return path which has been shown to produce instabilities in SLCs (13).

Recently, adaptive SLC (ASLC) was investigated for two VADs performing as a total artificial heart (TAH) (14). This controller used physiologically representative CLs and non-vertical linear return paths for both the LVAD and RVAD. This TAH-ASLC was adaptive and modified different combinations of the LVAD and RVAD CLs when an emergency haemodynamic situation was detected. Adaption triggering scenarios included pulmonary congestion, atrial suction, and insufficient pump flow. Proportional-integral control was used to modify the CLs until the controller alleviated the haemodynamic danger. Despite the impressive haemodynamic performance demonstrated by the TAH-ASCL, it was only implemented in a non-pulsatile setting. Emergency-only adaption is also hindered by hysteresis which leaves the CL set at an inappropriately high or low CL after an adaptive event has resolved. The controller then requires an adverse event of the opposite nature to begin further modifications of the CL, which may return to its resting value or even beyond, depending on the severity of the adverse event. Emergency only CL migration also allows for situations where following an emergency adaption, the controller can leave the VAD OP towards the periphery of the emergency event until the emergency resolves itself, or intervention occurs.

Most recently, the authors' published an immediate response BiVAD-SLC which used physiological CLs and a non-vertical linear return path for both LVAD and RVAD (13). This SLC demonstrated good controller stability, suction avoidance, and preload sensitivity but lacked an adaptive mechanism. This study expands the previously proposed BiVAD-SLC into a BiVAD adaptive SLC (ASLC). The ASLC includes an emergency response to alleviate adverse events immediately but also includes a novel sweet spot (SS) adaptive response which can slowly bring the controller OP back to within a predefined operating zone (SS zone). The clinician chooses the SS zone with considerations to maintaining patient comfort and quality of life. The SS controller can also help to prevent emergency response situations that are developing over prolonged periods and will reduce hysteresis introduced by the emergency response, as seen in other published ASLCs (12,14).

This study compared the performance of the developed ASLC, an SLC, and clinically used constant speed control (CSC) in a BiVAD supported physical mock circulation loop (MCL) to demonstrate the benefits of a sweet spot ALSC which maintains haemodynamics within predefined levels over a broader range of perturbations than SLC or CSC.

Methods

Starling-Like Control (Immediate Response)

A detailed description of the immediate response SLC is given elsewhere (13). Briefly, the immediate response SLC is based on the healthy heart's ability to regulate CO in response to changes in ventricular preload. SLC flow regulation is achieved by emulating the cardiac response curve as a CL (control line) and employing a fixed non-vertical linear return path to predict the required steady-state VAD output following changes in preload. The SLC regulates VAD speed (and therefore flow) to match the target flow as identified by the point of intersection of the CL and return path (Figure 2). In this study, the CL is given by the sigmoid equation (1) and (2) for the LVAD and RVAD respectively which were fitted mathematically using the generalised reduced gradient non-linear solving method

(Microsoft Excel 2010, Microsoft Corporation, Redmond, WA, USA, $R^2 > 0.99$,) to the cardiac response curves given by Guyton (2).

$$\overline{Q_{LVAD}}^{*} = \left(10.3 + \left(\frac{-10.3}{1 + \left(\frac{P_{LVED}}{7} \right)^{2.3}} \right) \right) \cdot SF_L \quad (1)$$

$$\overline{Q_{RVAD}}^{*} = \left(10.05 + \left(\frac{-10.05}{1 + \left(\frac{P_{RVED}}{3.2} \right)^{2.5}} \right) \right) \cdot SF_R \quad (2)$$

In (1) and (2), $\overline{Q_{LVAD}}^{*}$ and $\overline{Q_{RVAD}}^{*}$ are the target pump flows, P_{LVED} and P_{RVED} are the left and right end-diastolic pressures (indicating preload), and SF_L and SF_R are a scaling factors which modifies the preload sensitivity and maximum flow rate of the LVAD and RVAD CL respectively. In the case of immediate response SLC, the scaling factors are fixed values.

Deviations of the VAD OP from the CL results in modifications of pump speed (and therefore flow) which cause the OP to be iteratively stepped back along the return path until the OP intersects with the CL. An example of increases and decreases in preload is given in Figure 2.

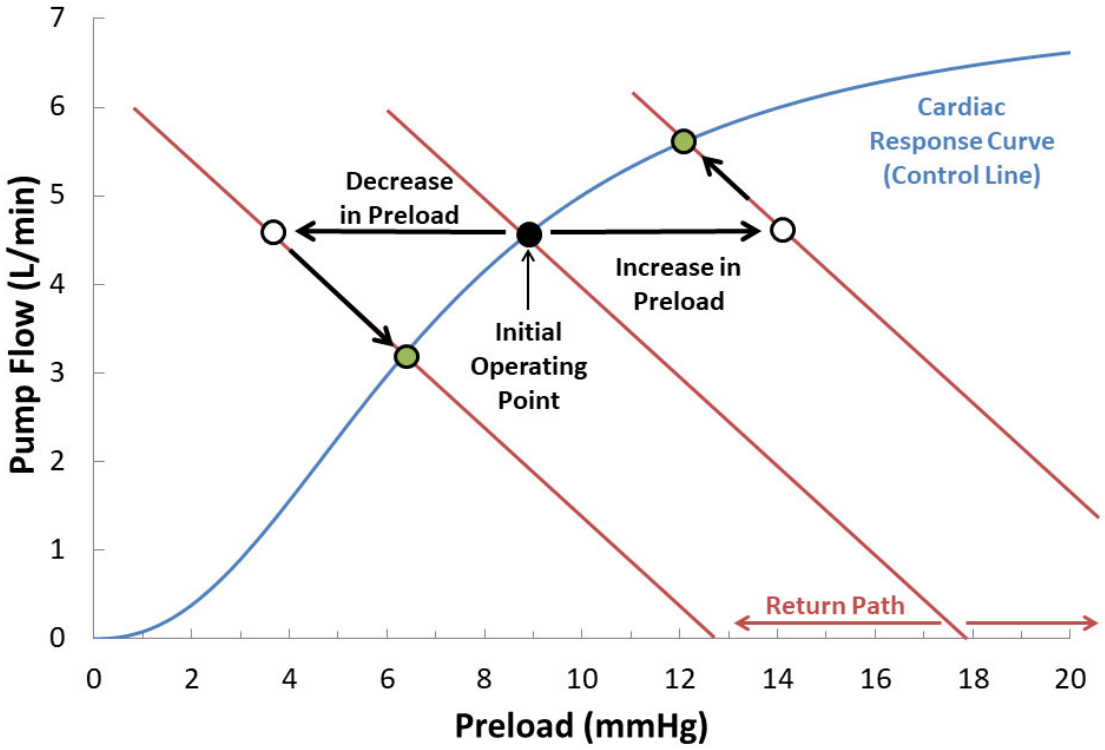

Figure 2: Immediate response Starling-like control uses control lines (CL) (to emulate the native cardiac response curves) and a return path to predict the required steady state pump flow. Deviations of the operating point (OP) from the control line (white circles) causes modifications in pump speed and flow which step the OP back along the return path until it intersects with the CL (green circles).

Proportional-integral control is used to minimise the error between the measured VAD flow $\overline{Q_{VAD}}$ and target $\overline{Q_{VAD}}^{*}$ on the CL by modifying pump speed. Using the return path allows for accurate prediction of $\overline{Q_{VAD}}^{*}$ and reduces the likelihood of significant overshoot or undershoot resulting in controller instability. The proportional-integral controllers which converge target flow and measured flow for the immediate response were tuned using a Ziegler-Nichols approach by inducing a step change of ± 1 L/min in the target proportional-integral controller (for example LVAD controller) while leaving the other proportional-integral controller (for example RVAD controller) in closed-loop with feedback from the SLC. The proportional-integral controllers were then optimised empirically to produce a step response of the immediate response with no overshoot and a settling time of no more than 20 seconds; these gains do not translate directly to the final ASLC response which is also determined by the SS adaption time (as explained below). The operating frequency of both proportional-integral controllers was 2 kHz.

The limitation of an immediate response SLC is that a single CL which is appropriate for rest will not be able to provide appropriate VAD flow for all circulatory states, for example, when the patient exercises.

Adaptive Starling-Like Control

Adaptive Starling-like control provides a solution to the limited flow adjustment capability of immediate response SLC by adapting the CL dynamically to meet a broader range of circulatory conditions; this applies particularly to high preloads when the CL asymptotes. The CL migrations can be achieved by dynamically modifying the scaling factor of the CL as defined in equations (1) and (2), which adjust both the preload sensitivity and maximum CO of the CL (slope of the line and height of the asymptote).

Because it is difficult to measure the nervous stimuli which cause adaption in the native heart, the ASLC instead uses clinician defined control boxes to facilitate CL migrations (Figure 3), as have been used in previously published ASLCs (12,14). The control box defines the upper and lower preload limits which, when exceeded, causes a CL migration to a higher or lower CL depending on which limit was violated. The control box also defines the absolute maximum and minimum VAD flow values which the clinician must set to ensure appropriate perfusion for all scenarios as well as preventing pump backflow.

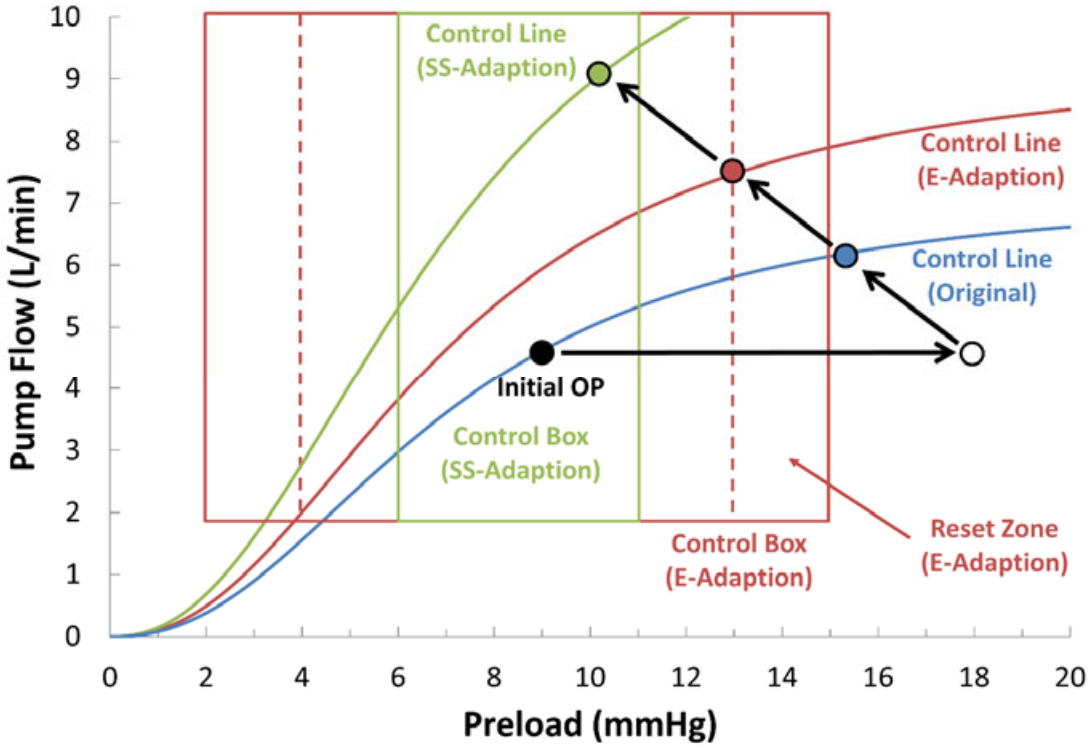

Figure 3: Adaptive Starling-like control (ASLC) uses control boxes (emergency (E) shown in red, sweet spot (SS) in green) to trigger control line migrations. In this example, the operating point (OP) increases drastically in preload, triggers an E adaption to the red control line, and then triggers a further SS adaption to the green control line. The dotted red line shows the reset zone for the E control box, while the reset zone for the SS control box is not drawn for simplicity. The return path has also been excluded but can be observed to have the same angle as the diagonal arrows.

The proposed ASLC consists of two adaptive mechanisms. The first is the emergency response which triggers CL migrations in situations where the patient is in imminent danger. The second mechanism is a novel SS response, which is used to keep the operating point inside a smaller predefined haemodynamic range (SS zone). The emergency response and SS response both use separate independent control boxes. Both control boxes employ variable reset zones (typically 1-2 mmHg) which help to prevent constant CL migrations ("hunting") from triggering (Figure 3). Afterload limits were also placed on the mean aortic pressure ($\overline{P_{AO}}$) and mean pulmonary artery pressure ($\overline{P_{PA}}$). These limits work by preventing further increases or decreases in pump speed once the upper or lower afterload limit has been

violated. Owing to the need for additional sensors, these limits are considered optional and can be turned off without affecting controller performance.

The emergency response triggers immediately once the preload moves outside the upper or lower limits and once the LVAD and RVAD are both converged to the CL (in a steady state). From the current OP which now rests outside of the control box, the controller "looks ahead", projecting the OP along the return path until a point of intersection occurs within the emergency reset limit (dotted line Figure 3). A new scaling factor which intersects the projected OP is then calculated trigonometrically using equations (3) and (4) which are algebraic variations of equation (1) and (2). The CL migration triggers and the OP is brought back to within the safe limits through adjustments in VAD flow. If the controller cannot find a point of intersection within the flow limits, it instead migrates to the highest or lowest CL which exists safely within the emergency flow limits.

$$SF_L = \left(10.03 + \left(\frac{-10.03}{1 + \left(\frac{P_{LVED}}{7}\right)^{2.3}} \right) \right) \cdot \frac{1}{\overline{Q_{LVAD}}^{*}} \tag{3}$$

$$SF_R = \left(10.05 + \left(\frac{-10.05}{1 + \left(\frac{P_{RVED}}{3.2}\right)^{2.5}} \right) \right) \cdot \frac{1}{\overline{Q_{RVAD}}^{*}} \tag{4}$$

The SS response uses a similar method of activation to the emergency response but does not require emergency preload levels to trigger. Instead, whenever the OP exceeds the SS limits, and both the LVAD and RVAD are converged with the CL, a user variable counter starts increasing. The controller will take ten evenly spaced preload samples within the counter period. Ten evenly spaced samples were chosen for this experiment to give good resolution of the preload within the counter time while not oversampling; however, this value can be modified as necessary. If the average of those ten samples exceeds the SS preload limits, the SS response will engage. Once the SS response is engaged another user

variable counter is used to trigger incremental increases or decreases in the CL scaling factor using proportional-integral control until the OP is back within the SS reset limits, or until the OP reaches either the flow or afterload limit, after which point the SS response will turn off. While the SS response is engaged, the scaling factor will only increment when both the LVAD and RVAD are converged with the CL, and in the steady state, this is done to ensure controller stability and prevent race conditions (whereby the controller would behave differently depending on whether the LVAD or RVAD settled first).

For this study, the upper and lower scaling factor limits for the LVAD and RVAD were set to 0.35 and 1.65 based on the upper and lower flow limit of the control box. The return path gradients were set to -1.96 L/min/mmHg and -0.84 L/min/mmHg for the LVAD and RVAD respectively, which were mathematically derived from the MCLs known parameters using equations as explained in previous works (15). The control box limits for this study (Table 1) were carefully chosen by engineers and a senior intensive care physician, to demonstrate the controller's capability to respond to a diverse range of physiological perturbations using only a single control box. In practice, the limits would be defined using the clinician's expertise and based on the patient's physiology, level of activity, and hospital-specific guidelines (such as intermittent valve opening). For brevity of experiments, the SS engage time was set to 30 seconds, while the SS increment timer triggered after 20 seconds in the steady state. Reset zones for the emergency and sweet spot responses were set to 1 mmHg. The gains for the SS scaling factor incremental proportional-integral controller were optimised manually. For both the LVAD and RVAD, different proportional and integral gains were used depending on whether the OP was in the upper or lower preload region due to the convergence of the CLs at low preloads. The PI gains for the scaling factors were optimised such that a step change in preload from 9 to 20 mmHg or conversely from 9 to 0 mmHg would take only six steps to return the OP to the SS zone.

Table 1: Haemodynamic limits for the ASLC used in these experiments.

P_{LVED}, P_{RVED} - left and right end-diastolic pressure; $\overline{Q_{LVAD}}$, $\overline{Q_{RVAD}}$ - mean left and right ventricular assist device flow; $\overline{P_{AO}}$ - mean aortic pressure; $\overline{P_{PA}}$ - mean pulmonary artery pressure.

Control Box Limits	LVAD	RVAD
Emergency Preload (mmHg)	$4 < P_{LVED} < 12$	$1 < P_{RVED} < 9$
Sweet Spot Preload (mmHg)	$6 < P_{LVED} < 10$	$3 < P_{RVED} < 7$
Flow Limits (L/min)	$2.5 < \overline{Q_{LVAD}} < 10.5$	$2.5 < \overline{Q_{RVAD}} < 10.5$
Afterload Limits (mmHg)	$65 < \overline{P_{AO}} < 110$	$10 < \overline{P_{PA}} < 25$

In-Vitro Experimental Setup

The ASLC was compared against SLC (which did not adapt and had no afterload limits), and clinically used CSC (constant speed control). A physical MCL was used to evaluate the controllers by simulating a variety of haemodynamic perturbations. The MCL is described in detail in (16,17). Briefly, the MCL models the pulmonary and systemic circulations. A Starling mechanism regulates the MCL LV and RV contractility based on end-diastolic volume through adjustments of the regulator supply voltage. Heart rate (HR) and systolic fraction can also be adjusted within the model. The MCL working fluid was a mixture of glycerol and water diluted to the same viscosity as blood at 3.4 cP (3.4 mPa·s). Pulmonary and systemic vascular resistances (PVR, SVR) are controlled independently through pneumatically actuated pinch valves (VMP025.03X.71, AKO UK, Northamptonshire, UK). The MCL was configured in a bi-ventricular heart failure scenario which was supported by two HeartWare HVADS (HeartWare Inc., Framingham, MA, USA) with the inlet cannulae in the LV and RV and the outlet cannulae in the aorta and pulmonary artery respectively. The RVAD was banded using a Ø 5.5 mm, 50 mm long 3D-printed restriction to compensate for the lower pressure observed in the pulmonary system (18). The VADs were run using a custom-built controller (DRV8312-C2-Dev-Kit, Texas Instruments Inc., TX, USA) which allows direct feedback control over the HVADs and provides an interface with the MCL software. The MCL

software model and ASLC were executed in a MATLAB/Simulink model (The MathWorks r2013b, Natick, MA, USA) at a running frequency of 2 kHz. The schematic of the mock loop is available in Figure 4, and a controller block diagram is available in Figure 5.

All data were acquired using a dSPACE 1103 (dSPACE, Paderborn, Germany), data were recorded at 2 kHz and down-sampled to 200 Hz for post-processing. All pressures were measured using silicone strain gauge transducers (PX181B-015C5V, Omega Engineering, Stamford, CT, USA). Systemic flow (Q_S) was measured using a magnetic inductive flow meter (Optiflux 1010C/D, Krohne, Duisburg, Germany). Pulmonary flow (Q_P), LVAD flow (Q_{LVAD}), and RVAD flow (Q_{RVAD}) were measured using clamp-on ultrasonic sensors (TS410-10PXL, Transonic Systems, Ithaca, NY, USA, for Q_{LVAD} and Q_{RVAD}, TS410-25PXL, Transonic Systems, for Q_P). Left and right end-diastolic pressures (P_{LVED}, P_{RVED}) were extracted from within the MCL model by taking LV and RV pressure readings prior to systole.

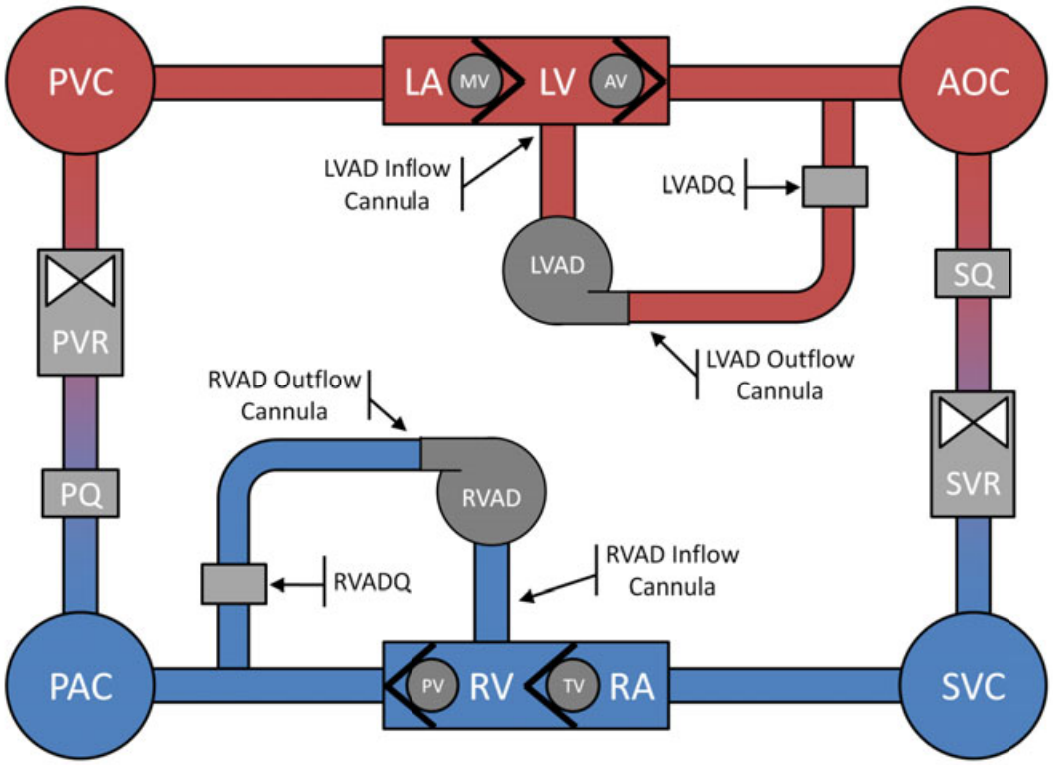

Figure 4: Schematic of the mock circulation loop (MCL) configured for biventricular support.

LA, RA - left and right atria; LV, RV - left and right ventricle; MV, AV, TV, PV - mitral, aortic, tricuspid, and pulmonary valves; AOC, SVC, PAC, PVC - aortic, systemic venous, pulmonary arterial, and pulmonary venous compliance chambers; SVR, PVR - systemic and pulmonary vascular resistance valves; SQ, PQ - systemic and pulmonary flow meters; LVAD,RVAD - left and right ventricular assist devices; LVADQ, RVADQ - LVAD and RVAD flow meters.

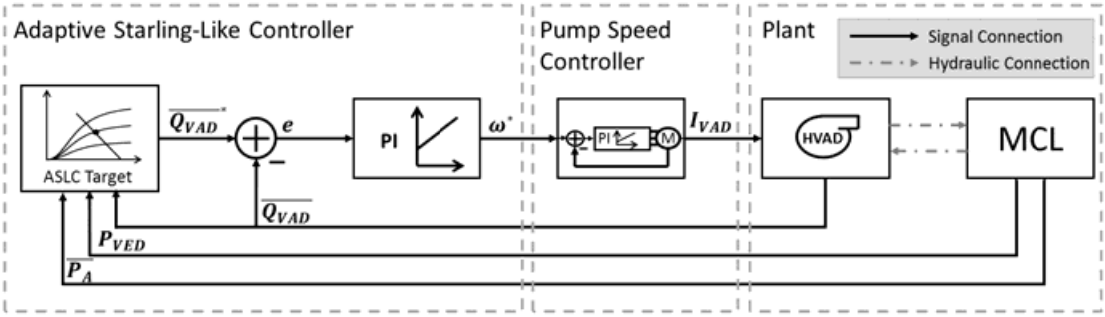

Figure 5: Adaptive Starling-like controller (ASLC) block diagram including ASLC, pump speed controller, and plant.

$\overline{Q_{VAD}}^*$ – target mean left or right ventricular assist device flow (VAD); $\overline{Q_{VAD}}$ – mean left or right VAD flow; P_{VED} – left or right end-diastolic ventricular pressure; $\overline{P_A}$ – mean aortic or pulmonary artery pressure; I_{VAD} – VAD current; ω* - target VAD speed; MCL – mock circulation loop.

Experimental protocol

The MCL was configured to simulate severe biventricular heart failure by setting the SVR and PVR to 1450 and 270 dyne · s · cm^{-5} respectively and adding 2 L of circulating fluid to simulate fluid retention prior to diuretics administration (19). Following the establishment of the heart failure haemodynamics (Table 2), the additional circulating fluid was removed, and SVR and PVR were returned to 1200 and 160 dyne · s · cm^{-5} respectively. The ASLC was then turned on at a fixed scaling factor of 0.82 (as used for SLC to produce the same baseline). The ASLC restored the cardiovascular haemodynamics to a healthy condition (Table 4). The pump speeds produced by the ASLC (and therefore SLC due to the same starting point) at the restored condition were also used for CSC to produce the same baseline for all experiments. The baseline HR was maintained at 80 beats per minute for both the unsupported and BiVAD restored conditions.

Four perturbations were introduced into the circulation, simulating exercise, slow wave sleep, fluid loading, and systemic hypertension. Each of the conditions was simulated by varying different MCL parameters including adding or removing circulating volume (to simulate variations in cardiac reserve), modifications in PVR, SVR, and HR, as well as variations in ventricular contractility through augmenting regulator voltage (Table 3). These conditions were chosen because they represent a diverse variety of possible patient conditions. The test values were set to physiologically relevant, albeit, extreme ranges to test the limits of the controller.

Table 2: Mock circulation loop haemodynamic parameters for heart failure (HF) and restored condition (RC) following biventricular assist device support.

CO – cardiac output; $\overline{P_{AO}}$ – mean aortic pressure; $\overline{P_{PA}}$ – mean pulmonary artery pressure; P_{LVED}, P_{RVED} – left and right end-diastolic pressure; SVR, PVR – systemic and pulmonary vascular resistance.

Haemodynamic Variable	CO (L/min)	$\overline{P_{AO}}$ (mmHg)	$\overline{P_{PA}}$ (mmHg)	P_{LVED} (mmHg)	P_{RVED} (mmHg)	SVR (dyne·s· cm^{-5})	PVR (dyne·s· cm^{-5})
Baseline (HF)	3.4	85.7	28.0	17.5	13.6	1450	270
Baseline (RC)	5.0	81.5	21.0	7.9	3.8	1200	160

Table 3: Clinical scenarios simulated on the mock circulation loop (MCL) detailing the physiological scenario, modified MCL parameters, values, and literature supporting the values.

SVR - systemic vascular resistance; PVR - pulmonary vascular resistance; HR -heart rate.

Clinical Scenario	Test Parameter	Values	Referenced Literature
Baseline (Restored Heart Failure at Rest)	SVR	1200 dyne·s·cm^{-5}	(13,20)
	PVR	160 dyne·s·cm^{-5}	
	HR	80 BPM	
Exercise	SVR	1200 → 700 dyne·s·cm^{-5}	(14,21,22)
	PVR	160 → 70 dyne·s·cm^{-5}	
	HR	80 → 100 BPM	
	Volume	+700 mL	
	Contractility	+10%	
Slow Wave Sleep	SVR	1200 → 1080 dyne·s·cm^{-5}	(20,23)
	HR	80 → 60 BPM	

	Volume	-350 mL	
	Contractility	-15%	
Fluid Loading	Volume	+650 mL	-
Systemic Hypertension	SVR	1200 → 3000 dyne·s·cm^{-5}	(20)

The pattern of simulation was to have 10 seconds of baseline data followed by an onset of the test condition over 60 seconds. The test was held for a period of either 5 or 7.5 minutes depending on the severity of the perturbation. The test condition was then returned to baseline over 60 seconds and held for another period of either 5 or 7.5 minutes to allow controller settling. Each perturbation was conducted once for each ASLC, SLC, and CSC. Each controller was evaluated on its ability to remain within the clinician defined SS zone, thus avoiding ventricular suction (P_{LVED}, P_{RVED} < 0 mmHg) and congestion (P_{LVED}, P_{RVED} > 15 mmHg) (24) while maintaining safe afterload levels (65 < $\overline{P_{AO}}$ < 110 mmHg, 10 < $\overline{P_{PA}}$ < 25 mmHg).

Results

The primary findings from each experiment are outlined in their respective subsections. Figure 6 and Figure 7 detail the important haemodynamics from each controller. The figures for the remaining experiments are omitted in the main text for brevity but are available in the supplemental materials. A detailed comparison of the steady-state haemodynamic values for each experiment is detailed in Table 4. The scaling factors during each experiment are presented in the supplemental materials.

Exercise

During exercise, ASLC triggered CL migrations to higher curves for both LVAD and RVAD due to the increase in preload, which allowed the controller to increase CO ($\overline{Q_S}$ and $\overline{Q_P}$ - matched due to the lack of a bronchial shunt) to 10.1 L/min, with no flow through the semilunar valves. The SLC produced a moderate increase in $\overline{Q_S}$ and $\overline{Q_P}$ up to 7.3 L/min (with

aortic valve flow - $\overline{Q_{AV}}$ of 0.7 L/min, and no pulmonary valve flow - $\overline{Q_{PV}}$), while CSC increased flow to only 6.2 L/min ($\overline{Q_{AV}}$ of 0.8 L/min, no $\overline{Q_{PV}}$). The ASLC unloaded the LV and RV adequately, with P_{LVED} at 8.5 mmHg and P_{RVED} at 6.8 mmHg, an improvement over SLC (13.1 and 8.1 mmHg), and CSC (10.2 and 10.2 mmHg). Mean aortic pressure ($\overline{P_{AO}}$) was increased to a physiologically representative level by ASLC, rising from 81 to 99.8 mmHg. SLC and CSC both produced a fall in $\overline{P_{AO}}$ to 74.2 and 65.8 mmHg respectively, owing to the drop in MCL SVR coupled with each controller's inability to provide adequate flow rates. ASLC remained within the SS zone for both LVAD and RVAD, although during the transition away from exercise $\overline{P_{AO}}$ did transiently exceed the afterload limit. Meanwhile, SLC and CSC did not remain in the SS with both controllers exceeding the high preload limit for LVAD and RVAD. CSC also exceeded the upper emergency preload limit for the RVAD indicating the potential for systemic congestion. It can be noted that unlike SLC and CSC, ASLC does not return to the starting haemodynamic levels following return to baseline if a CL adaption has occurred. This is acceptable provided the controller OP remains within the SS zone.

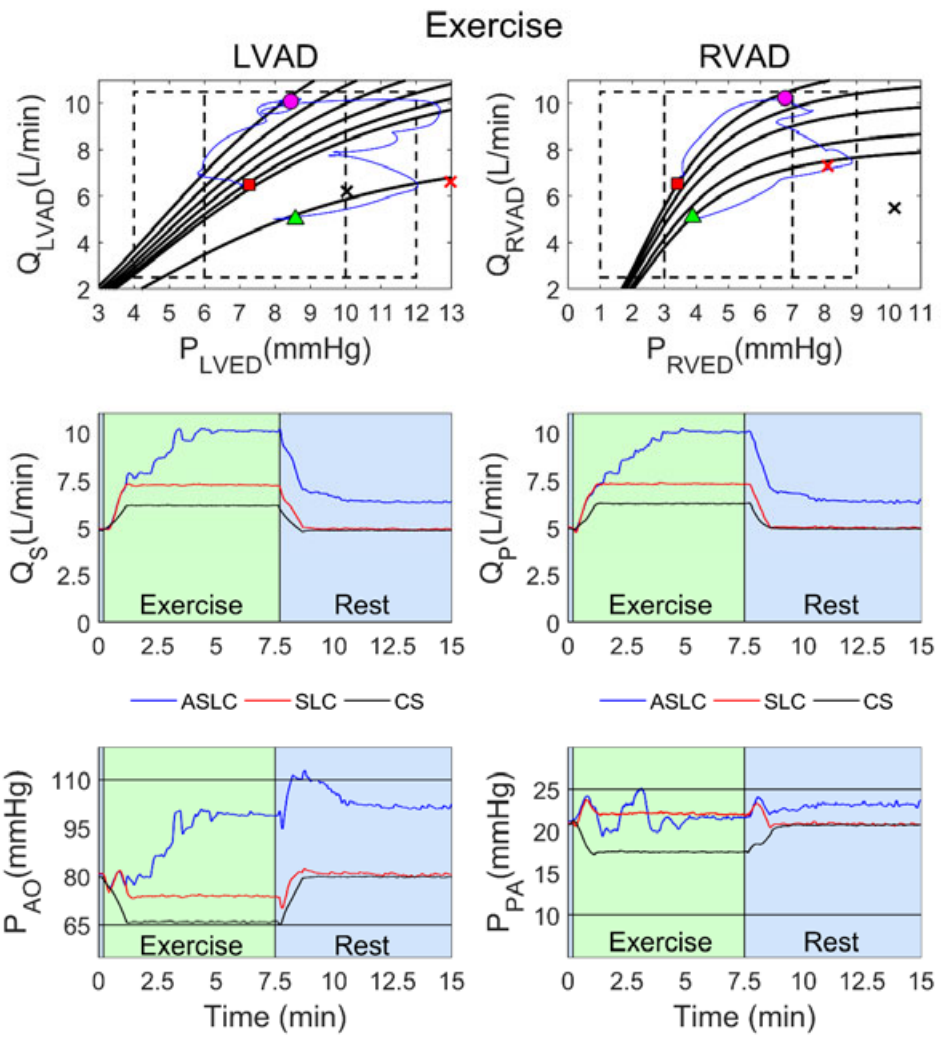

Figure 6: Results for exercise condition for the adaptive Starling-like controller (ASLC) showing the path of the operating point (OP) (top), systemic and pulmonary flow rates for all controllers (middle), and arterial pressures for all controllers with upper and lower afterload limits (bottom).

SLC – Starling-like controller; CSC – constant speed control; QLVAD, QRVAD - mean left and right ventricular assist device flow; PLVED, PRVED - left and right ventricular end-diastolic pressure; Q_S, Q_P - mean pulmonary and systemic flow; PAO, PPA - mean aortic and pulmonary artery pressure; green triangle - ASLC OP starting point; magenta circle - ASLC OP condition steady state; red square - ASLC OP end point; Red X – SLC steady-state OP point; Black X – CSC steady-state OP point.

Sleep

During sleep, ASLC triggered CL migrations to a lower CL for the LVAD due to the reduction in preload. Owing to its higher preload sensitivity compared to the LVAD, the RVAD could reduce VAD flow to adequate levels without requiring a CL adaption. After migrating to a

lower LVAD CL, CO reduced to 4.5 L/min. This reduction encouraged an increase in $\overline{Q_{AV}}$ to 2.1 L/min. Similarly, SLC produced a CO of 4.6 L/min with 1.3 L/min $\overline{Q_{AV}}$. Conversely, CSC slightly increased the CO to 5.1 L/min with no flow through the semilunar valves. Both ASLC and CSC reduced $\overline{P_{AO}}$ to physiologically representative levels 65.8 and 67 mmHg respectively, whereas CSC maintained relatively constant $\overline{P_{AO}}$ at 74.5 mmHg. The increase in CO and decrease in $\overline{P_{AO}}$ observed with CSC were attributed to the pressure head-flow characteristics of the VAD which ascribe an increase in flow with a decrease in pressure if outlet pressure is reduced (via reduction in SVR) and VAD speed is maintained. ASLC remained within the SS zone for both LVAD and RVAD. SLC was below the lower LVAD SS preload limit (P_{LVED} of 5.9 mmHg). CSC LVAD did not remain within the LVAD SS zone (P_{LVED} of 5.3 mmHg).

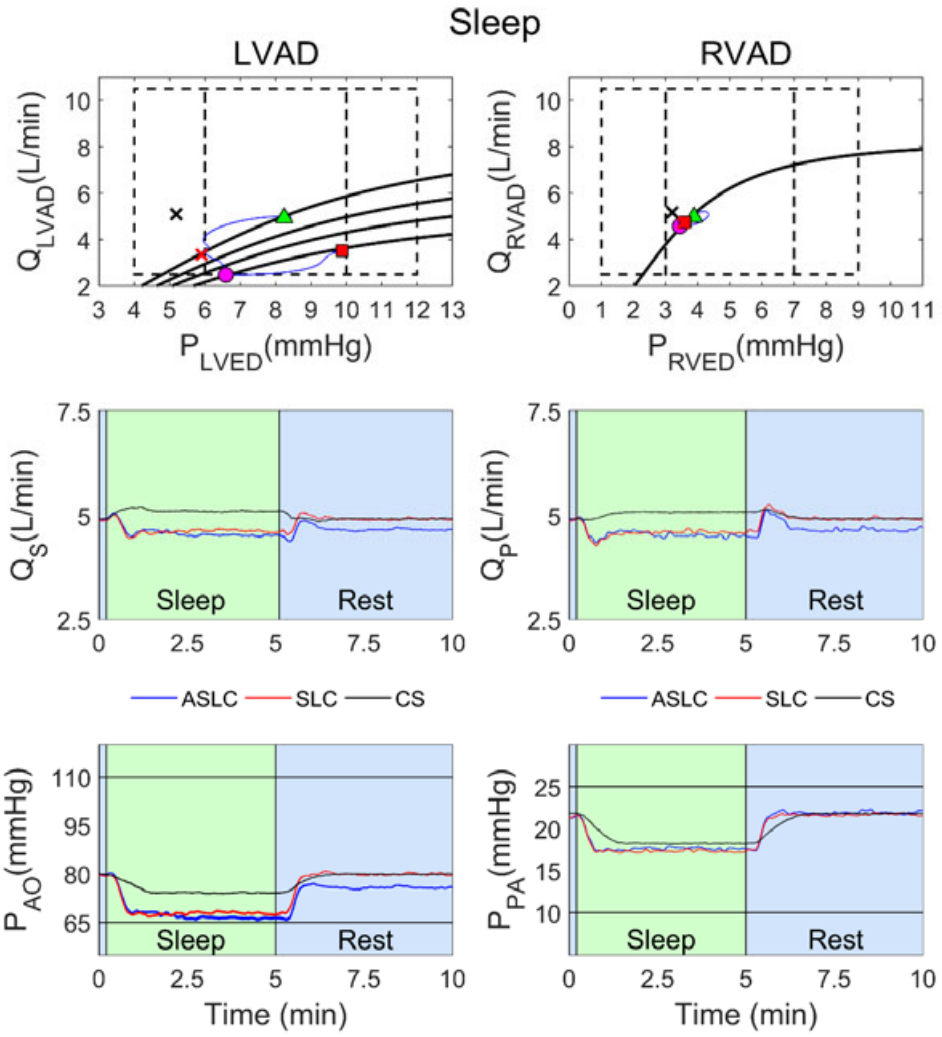

Figure 7: Results for sleep condition for the adaptive Starling-like controller (ASLC) showing the path of the operating point (OP) (top), systemic and pulmonary flow rates for all controllers (middle), and arterial pressures for all controllers with upper and lower afterload limits (bottom).

SLC – Starling-like controller; CSC – constant speed control; QLVAD, QRVAD - mean left and right ventricular assist device flow; PLVED, PRVED - left and right ventricular end-diastolic pressure; Q_S, Q_P - mean pulmonary and systemic flow; PAO, PPA - mean aortic and pulmonary artery pressure; green triangle - ASLC OP starting point; magenta circle - ASLC OP condition steady state; red square - ASLC OP end point; Red X – SLC steady-state OP point; Black X – CSC steady-state OP point

Fluid Loading

During fluid loading, ASLC triggered CL migrations to higher curves for the LVAD in response to the increased preload, while the RVAD had adequate preload sensitivity to adjust flow without a CL adaption. ASLC and SLC produced similar CO at 6.3 and 6.4 L/min respectively. CSC CO remained relatively constant at 5.1 L/min with 0.3 L/min $\overline{Q_{AV}}$. There was variation in mean pulmonary artery pressure ($\overline{P_{PA}}$) between the controllers with ASLC reaching the upper limit of 25 mmHg, after which the controller did not continue to increase RVAD flow. This is an improvement over SLC which, with no limit, increased $\overline{P_{PA}}$ to 28.4 mmHg, beyond the predefined safe levels. Meanwhile, CSC $\overline{P_{PA}}$ reached 23.4 mmHg. Increased LV unloading was observed with ASLC (P_{LVED} of 9.2 mmHg) compared to SLC (P_{LVED} of 12.0 mmHg) due to the increased load coming from the un-limited SLC-RVAD. CSC also resulted in a high LV preload (P_{LVED} of 10.6 mmHg. ASLC remained in the SS for both LVAD and RVAD, whereas SLC and CSC strayed outside for both LVAD (high preload SLC and CSC) and RVAD (high afterload for SLC and high preload for CSC).

Systemic Hypertension

During simulated systemic hypertension, ASLC decreased the RVAD CL in response to the reduced RV preload, which resulted in a CO of 3.7 L/min. The SLC CO reduced to 4.3 L/min, while CSC reduced CO to 3.6 L/min with 1.8 L/min $\overline{Q_{AV}}$, due to the increased ventricular loading. With no flow balancing mechanism, CSC resulted in significant LV loading (P_{LVED} of 25 mmHg), while also experiencing RV suction (P_{RVED} of -3.5 mmHg). $\overline{P_{AO}}$ increased above the defined safe limit for all three controllers at 144, 168.3 and 134.7 mmHg for ASLC, SLC and CSC respectively. CSC also reached $\overline{P_{PA}}$ levels above the defined threshold at 35.7 mmHg, whereas ASLC and SLC remained within the acceptable range (17.0 and 18.5 mmHg respectively). Despite the large differences in $\overline{P_{AO}}$ ASLC and SLC remained within the SS preload limits for LVAD and RVAD, although neither could maintain LV afterload within the defined ranged. CSC was outside of the SS for both LVAD (high preload, high afterload) and RVAD (RV suction, high afterload).

Tabulated

Table 4: Steady-state haemodynamics for each controller during the simulated conditions. Green cells are values within the sweet spot limits while red cells fall outside the sweet spot limits.

ASLC- adaptive Starling-like control; SLC – Starling-like control; CSC– constant speed; HF - heart failure condition; RC – restored haemodynamic condition; CO ($\overline{Q_S}$ and $\overline{Q_P}$) – matched systemic and pulmonary flows; $\overline{P_{AO}}$ – mean aortic pressure; $\overline{P_{PA}}$ – mean pulmonary artery pressure; P_{LVED}, P_{RVED} – left and right end-diastolic pressure; $\overline{Q_{AV}}$, $\overline{Q_{PV}}$ – mean aortic and pulmonary valve flow; ω_{LVAD}, ω_{RVAD} – left and right ventricular assist device speed.

Haemodynamic Variable	CO (L/min)	$\overline{P_{AO}}$ (mmHg)	$\overline{P_{PA}}$ (mmHg)	P_{LVED} (mmHg)	P_{RVED} (mmHg)	$\overline{Q_{AV}}$ (L/min)	$\overline{Q_{PV}}$ (L/min)	ω_{LVAD} (rpm)	ω_{RVAD} (rpm)
Baseline (HF)	3.4	85.7	28.0	17.5	13.6	3.4	3.4	-	-
Baseline (RC)	5.0	81.5	21.0	7.9	3.8	0	0	2460	2240
Exercise (ASLC)	10.1	99.8	21.8	8.5	6.8	0	0	3670	3610
Exercise (SLC)	7.3	74.2	22.1	13.1	8.1	0.7	0	2560	2890
Exercise (CSC)	6.2	65.8	17.6	10.2	10.2	0	0.8	2460	2240
Sleep (ASLC)	4.5	65.8	17.7	6.6	3.4	2.1	0	2040	2040
Sleep (SLC)	4.6	67	17.2	5.9	3.7	1.3	0	2150	2070
Sleep (CSC)	5.1	74.5	18.2	5.3	3.2	0	0	2460	2240
Fluid Loading (ASLC)	6.3	102.0	25.0	9.2	6.6	0	0	2960	2600
Fluid Loading (SLC)	6.4	104.9	28.4	12.0	5.4	0	0	2940	2720
Fluid Loading (CSC)	5.1	85.8	23.4	10.6	7.0	0.3	0	2460	2240
Hypertension (ASLC)	3.7	144	17	7.3	3.9	0	0	3190	1750
Hypertension (SLC)	4.3	168.3	18.5	7.7	3.4	0	0	3470	1990
Hypertension (CSC)	3.6	134.7	35.7	25	-3.5	1.8	0	2460	2240

Discussion

This study investigated an ASLC which has an emergency adaptive response and a novel SS adaptive response. ASLC was compared in a MCL against SLC and clinically used CSC. The primary aim of the ASLC is to keep the operating point within the predefined SS zone. Despite extreme changes to the simulated patient state, the ASLC was able to maintain the OP within the SS zone in three out of four simulated scenarios and was able to avoid left and right ventricular suction and pulmonary and systemic congestion during all scenarios. ASLC was unable to maintain the OP within the SS zone during simulated systemic hypertension where it exceeded the afterload limits. While afterload limits can help the ASLC to manage the risk between suction and congestion, typically, in heart failure patients, afterload is instead managed medically - especially in the case of prolonged systemic hypertension which typically develops slowly over time (25). Meanwhile, SLC and CSC could not maintain the OP within the SS zone for any of the simulated scenarios, and CSC entered right ventricular suction during simulated systemic hypertension.

These results are similar to those found in a previously investigated ASLC-TAH (14), which demonstrated that SLC, with its single CL, cannot provide optimal support for all possible physiological states. Interestingly, during exercise the ASLC-TAH increased LVAD scaling factor while decreasing RVAD scaling factor, this resulted in a CO of 8.4 L/min, a left atrial pressure of 17.5 mmHg, and a right atrial pressure of 9.6 mmHg, which may not represent adequate unloading of the left atrium. By comparison, the ASLC presented in this study produced a higher CO of 10.1 L/min, while also having lower preloads in the left and right ventricles (P_{LVED} of 8.5 and P_{RVED} of 6.8) during a more intense simulated exercise than that presented in the ASLC-TAH paper. Given that neither ventricles were ejecting during exercise, the reduced preloads presented here by the ASLC are likely given by the increase of both the LVAD and RVAD scaling factors, resulting in more aggressive unloading and higher CO.

Several benefits of including an SS response to the ASLC have been demonstrated. The foremost being that the SS response can modify the CL to keep the patient in a predefined range without the need for an emergency event to occur. The SS response has the additional benefit of overcoming two limitations associated with an emergency response only ASLC. The first limitation is that after an emergency CL migration occurs, the OP will still be left out on the periphery of the emergency event until the event is resolved (returned to rest) or intervention is sought. The SS-ASLC eradicates this limitation by continually trying to bring the OP to back within the predefined SS zone. The second limitation is hysteresis, which occurs in an emergency only ASLC after an emergency CL migration has occurred. The hysteresis is introduced because the emergency only ASLC will require an opposite emergency event to return to the original 'rest' CL, or beyond, depending on the severity of the emergency. Although the SS-ASLC still has inherent hysteresis, it only requires a smaller inverse event to return to a resting CL. The inverse scenario will reside on the opposite side of the SS zone and should occur naturally as the patient returns to their resting state or following medical intervention. Advanced solutions such as model predictive control, or additional measured parameters (like heart rate) may be used in the future for eliminating hysteresis from ASLC; however, these methods will need to be tested thoroughly to ensure improvement in controller performance outweighs the additional controller complexity.

One limitation of the ASLC is that it takes a long time to reach steady-state – particularly when multiple jumps are required to return the OP to the SS zone. This is demonstrated during exercise where the ASLC takes much longer to settle compared to SLC and CSC. Transient overshoots in both pressure and flow for the ASLC were also recorded, which are not present for SLC and CSC. The overshoots are due to a delay in the redistribution of fluid from the pulmonary and systemic circuits following a sudden increase in either LVAD or RVAD flow after CL adaption. The excessive transient $\overline{P_{AO}}$ is of particular concern and may be harmful to the patient. These limitations may be mitigated by pre-empting the eventual steady state condition and adapting both the LVAD and RVAD CLs simultaneously resulting in a smoother and more rapid steady state. Further experiments will be required to determine if the benefits of simultaneous adaption outweigh the added controller complexity.

The major technical limitation of this and many other physiological controllers is the lack of clinically available, reliable, implantable pressure transducers. In this study, ASLC used two pressure sensors and one flow sensor for each VAD. For BiVAD control, this would require six implantable sensors, which is a significant level of instrumentation. Implantable VAD flow sensors are clinically available, though their accuracy is uncertain (26) and they have not seen widespread clinical uptake. As it stands, the ASLC only measures VAD flow and does not take into account any output through the semilunar valves. Previous in-vitro studies have demonstrated that there may be a difference in the SLC response based on the opening status of the semilunar valve (13,27,28). Therefore, it would be ideal to be able to measure both the VAD flow and native ventricular outflow. It is also worth noting that implantable continuous pressure sensors are currently only investigational but may be clinically viable in the not-too-distant future and will likely be essential to the clinical adoption of any sufficiently sophisticated physiological controller (29,30).

The other major limitation of this study was the use of an MCL for evaluation. MCLs allow for rapid evaluations of physiological controllers but do not mimic many biological processes. In this study, the lack of autoregulation of the SVR and PVR due to the absent baroreflex may have implications for controller performance, especially the efficacy of the afterload limits. Therefore, further testing of the ASLC in an in-vivo model is required.

Further in-vivo work will be conducted to outline clinical guidelines for how to set the limits for the control boxes depending on the patient's physiology, level of activity, and level of disease. It is likely that the attending clinician would initially have the adaptive responses turned off in a critical care setting and would instead adjust the scaling factor of the CL manually as part of their routine patient management. When the patient is later discharged from hospital care the attending clinician would then set the control box limits based on the patient needs and this box might be updated intermittently as the patient recovers further, as part of their regular clinical management. Allowing the clinician to have a high level of control over the ASLC will be an essential part of the controller decision-making process to ensure the best patient outcomes given the particular situation of each patient. A high level

of clinician input may also help to alleviate some of the hesitance towards clinical adoption of a physiological controller such as ASLC.

Conclusion

ASLC maintained haemodynamics within the predefined levels over a broader range of circulatory states compared to SLC and CSC. Further investigation into removing hysteresis and guidelines for setting the control box limits will be essential for addressing the clinical applicability of ASLC. However, the potential for ASLC has been demonstrated in-vitro, and clinical translation of this kind of adaptive controller can help to improve for patient safety and quality of life, especially in the more active outpatient cohort.

References

1. Starling EH, Visscher MB. The Regulation of the Energy Output of the Heart. J Physiol. 1926;62:243–61.
2. Guyton AC. Determination of cardiac output by equating venous return curves with cardiac response curves. Physiol Rev. 1955;35(1):123–9.
3. SARNOFF SJ. Myocardial contractility as described by ventricular function curves; observations on Starling's law of the heart. Physiol Rev [Internet]. 1955;35(1):107–22. Available from: http://www.ncbi.nlm.nih.gov/pubmed/14356923
4. Salamonsen RF, Mason DG, Ayre PJ. Response of Rotary Blood Pumps to Changes in Preload and Afterload at a Fixed Speed Setting Are Unphysiological When Compared With the Natural Heart. Artif Organs. 2011;35(3):47–53.
5. Fukamachi K, Shiose A, Massiello A, Horvath DJ, Golding L a R, Lee S, et al. Preload sensitivity in cardiac assist devices. Ann Thorac Surg. 2013 Jan;95(1):373–80.
6. Saito S, Sakaguchi T, Miyagawa S, Yoshikawa Y, Yamauchi T, Ueno T, et al. Biventricular support using implantable continuous-flow ventricular assist devices. J Hear Lung Transplant [Internet]. 2011;30(4):475–8. Available from: http://dx.doi.org/10.1016/j.healun.2010.11.013
7. Pauls JP, Stevens MC, Bartnikowski N, Fraser JF, Gregory SD, Tansley G. Evaluation of Physiological Control Systems for Rotary Left Ventricular Assist Devices: An In-Vitro Study. Ann Biomed Eng [Internet]. 2016;44(8):2377–87. Available from: http://link.springer.com/10.1007/s10439-016-1552-3
8. Tchantchaleishvili V, Luc JGY, Cohan CM, Phan K, Hübbert L, Day SW, et al. Clinical Implications of Physiologic Flow Adjustment in Continuous-Flow Left Ventricular Assist Devices. ASAIO J [Internet]. 2017;63(3):241–50. Available from:

http://insights.ovid.com/crossref?an=00002480-900000000-99177

9. Pauls JP, Stevens MC, Schummy E, Tansley G, Fraser JF, Timms D, et al. In Vitro Comparison of Active and Passive Physiological Control Systems for Biventricular Assist Devices. Ann Biomed Eng [Internet]. 2016 May 18;44(5):1370–80. Available from: http://link.springer.com/10.1007/s10439-015-1425-1

10. Mansouri M, Salamonsen RF, Lim E, Akmeliawati R, Lovell NH. Preload-Based Starling-Like Control for Rotary Blood Pumps: Numerical Comparison with Pulsatility Control and Constant Speed Operation. PLoS One. 2015;10(4):1–16.

11. Petrou A, Lee J, Dual S, Ochsner G, Meboldt M, Schmid Daners M. Standardized Comparison of Selected Physiological Controllers for Rotary Blood Pumps: In Vitro Study. Artif Organs [Internet]. 2018 Mar;42(3):29–42. Available from: http://doi.wiley.com/10.1111/aor.12999

12. Gaddum NR, Timms DL, Stevens M, Mason D, Lovell N, Fraser JF. Comparison of Preload-Sensitive Pressure and Flow Controller Strategies for a Dual Device Biventricular Support System. Artif Organs. 2012;36(3):256–65.

13. Stephens AF, Stevens MC, Gregory SD, Kleinheyer M, Salamonsen RF. In Vitro Evaluation of an Immediate Response Starling-Like Controller for Dual Rotary Blood Pumps. Artif Organs [Internet]. 2017 Oct;41(10):911–22. Available from: http://doi.wiley.com/10.1111/aor.12962

14. Ng BC, Smith PA, Nestler F, Timms D, Cohn WE, Lim E. Application of Adaptive Starling-Like Controller to Total Artificial Heart Using Dual Rotary Blood Pumps. Ann Biomed Eng [Internet]. 2017 Mar 19;45(3):567–79. Available from: http://link.springer.com/10.1007/s10439-016-1706-3

15. Stephens AF, Gregory SD, Salamonsen RF. The Importance of Venous Return in Starling-Like Control of Rotary Ventricular Assist Devices. Artif Organs [Internet]. 2018 Nov 9;Accepted. Available from: http://doi.wiley.com/10.1111/aor.13342

16. Gregory SD, Stevens M, Timms D, Pearcy M. Replication of the Frank-Starling response in a mock circulation loop. In: Proceedings of the Annual International Conference of the IEEE Engineering in Medicine and Biology Society, EMBS. 2011. p. 6825–8.

17. Timms DL, Gregory SD, Greatrex NA, Pearcy MJ, Fraser JF, Steinseifer U. A Compact Mock Circulation Loop for the In Vitro Testing of Cardiovascular Devices. Artif Organs. 2011;35(4):384–91.

18. Timms D, Gude E, Gaddum N, Lim E, Greatrex N, Wong K, et al. Assessment of right pump outflow banding and speed changes on pulmonary hemodynamics during biventricular support with two rotary left ventricular assist devices. Artif Organs. 2011;35(8):807–13.

19. Muthiah K, Humphreys DT, Robson D, Dhital K, Spratt P, Jansz P, et al. Longitudinal structural, functional, and cellular myocardial alterations with chronic centrifugal continuous-flow left ventricular assist device support. J Hear Lung Transplant [Internet]. 2017;36(7):722–31. Available from: http://dx.doi.org/10.1016/j.healun.2016.05.017

20. Guyton AC, Hall JE. “Textbook Of Medical Physiology.” 11th ED. Guyton AC, Hall JE, editors. Elsevier Saunders. Pennsylvania: Elsevier Saunders; 2006. 1–1116 p.

21. Epstein SE, Beiser GD, Stampfer M, Robinson BF, Braunwald E. Characterization of the circulatory response to maximal upright exercise in normal subjects and patients with heart disease. Circulation [Internet]. 1967 Jun 1;35(6):1049–62. Available from:

http://circ.ahajournals.org/cgi/doi/10.1161/01.CIR.35.6.1049

22. Pauls JP. Development of a Passive Control System for Ventricular Assist Devices. Griffith University; 2017.

23. Coote JH. Respiratory and circulatory control during sleep. J Exp Biol [Internet]. 1982 Oct;100(1):223–44. Available from: http://www.ncbi.nlm.nih.gov/pubmed/6757369

24. Boston JR, Antaki JF, Simaan MA. Hierarchical control of heart-assist devices. IEEE Robot Autom Mag. 2003;10(1):54–64.

25. Slaughter MS, Pagani FD, Rogers JG, Miller LW, Sun B, Russell SD, et al. Clinical management of continuous-flow left ventricular assist devices in advanced heart failure. J Heart Lung Transplant [Internet]. 2010;29(4 Suppl):S1–39. Available from: http://dx.doi.org/10.1016/j.healun.2010.01.011

26. Banerjee D, Dutt D, Duclos S, Sallam K, Wheeler M, Ha R. Simultaneous ramp right heart catheterization and echocardiography in a ReliantHeart left ventricular assist device. World J Cardiol [Internet]. 2017;9(1):55–9. Available from: http://www.wjgnet.com/1949-8462/full/v9/i1/55.htm

27. Salamonsen RF, Lim E, Gaddum N, Alomari A-HHH, Gregory SD, Stevens M, et al. Theoretical Foundations of a Starling-Like Controller for Rotary Blood Pumps. Artif Organs. 2012;36(9):787–96.

28. Gaddum NR, Stevens M, Lim E, Fraser J, Lovell N, Mason D, et al. Starling-like flow control of a left ventricular assist device: In vitro validation. Artif Organs. 2014;38(3):46–56.

29. Starr P, Bartels K, Agrawal CM, Bailey S. A thin-film pressure transducer for implantable and intravascular blood pressure sensing. Sensors Actuators, A Phys [Internet]. 2016;248:38–45. Available from: http://dx.doi.org/10.1016/j.sna.2016.06.035

30. Brancato L, Keulemans G, Verbelen T, Meyns B, Puers R. An implantable intravascular pressure sensor for a ventricular assist device. Micromachines. 2016;7(8):1–17.

Figure Captions

Figure 8: The Starling response is intrinsic to the heart and can be characterised by cardiac output and venous return functions (solid lines). An extrinsic response also exists which modifies the preload sensitivity of the heart (dotted lines). CRC – cardiac response curve.

Figure 9: Immediate response Starling-like control uses control lines (CL) (to emulate the native cardiac response curves) and a return path to predict the required steady state pump flow. Deviations of the operating point (OP) from the control line (white circles) causes modifications in pump speed and flow which step the OP back along the return path until it intersects with the CL (green circles).

Figure 10: Adaptive Starling-like control (ASLC) uses control boxes (emergency (E) shown in red, sweet spot (SS) in green) to trigger control line migrations. In this example, the operating point (OP) increases drastically in preload, triggers an E adaption to the red control line, and then triggers a further SS adaption to the green control line. The dotted red line shows the reset zone for the E control box, while the reset zone for the SS control box is not drawn for simplicity. The return path has also been excluded but can be observed to have the same angle as the diagonal arrows.

Figure 11: Schematic of the mock circulation loop (MCL) configured for biventricular support.

LA, RA - left and right atria; LV, RV - left and right ventricle; MV, AV, TV, PV - mitral, aortic, tricuspid, and pulmonary valves; AOC, SVC, PAC, PVC - aortic, systemic venous, pulmonary arterial, and pulmonary venous compliance chambers; SVR, PVR - systemic and pulmonary vascular resistance valves; SQ, PQ - systemic and pulmonary flow meters; LVAD,RVAD - left and right ventricular assist devices; LVADQ, RVADQ - LVAD and RVAD flow meters.

Figure 12: Adaptive Starling-like controller (ASLC) block diagram including ASLC, pump speed controller, and plant.

$\overline{Q_{VAD}}^{*}$ – target mean left or right ventricular assist device flow (VAD); $\overline{Q_{VAD}}$ – mean left or right VAD flow; P_{VED} – left or right end-diastolic ventricular pressure; $\overline{P_A}$ – mean aortic or pulmonary artery pressure; I_{VAD} – VAD current; ω^{*} - target VAD speed; MCL – mock circulation loop.

Figure 13: Results for exercise condition for the adaptive Starling-like controller (ASLC) showing the path of the operating point (OP) (top), systemic and pulmonary flow rates for all controllers (middle), and arterial pressures for all controllers with upper and lower afterload limits (bottom).

SLC – Starling-like controller; CSC – constant speed control; QLVAD, QRVAD - mean left and right ventricular assist device flow; PLVED, PRVED - left and right ventricular end-diastolic pressure; Q_S, Q_P - mean pulmonary and systemic flow; PAO, PPA - mean aortic and pulmonary artery pressure; green triangle - ASLC OP starting point; magenta circle - ASLC OP condition steady state; red square - ASLC OP end point; Red X – SLC steady-state OP point; Black X – CSC steady-state OP point.

Figure 14: Results for sleep condition for the adaptive Starling-like controller (ASLC) showing the path of the operating point (OP) (top), systemic and pulmonary flow rates for all controllers (middle), and arterial pressures for all controllers with upper and lower afterload limits (bottom).

SLC – Starling-like controller; CSC – constant speed control; QLVAD, QRVAD - mean left and right ventricular assist device flow; PLVED, PRVED - left and right ventricular end-diastolic pressure; Q_S, Q_P - mean pulmonary and systemic flow; PAO, PPA - mean aortic and pulmonary artery pressure; green triangle - ASLC OP starting point; magenta circle - ASLC OP condition steady state; red square - ASLC OP end point; Red X – SLC steady-state OP point; Black X – CSC steady-state OP point

Table Captions

Table 5: Haemodynamic limits for the ASLC used in these experiments.

P_{LVED}, P_{RVED} - left and right end-diastolic pressure; $\overline{Q_{LVAD}}$, $\overline{Q_{RVAD}}$ - mean left and right ventricular assist device flow; $\overline{P_{AO}}$ - mean aortic pressure; $\overline{P_{PA}}$ - mean pulmonary artery pressure.

Table 6: Mock circulation loop haemodynamic parameters for heart failure (HF) and restored condition (RC) following biventricular assist device support.

CO – cardiac output; $\overline{P_{AO}}$ – mean aortic pressure; $\overline{P_{PA}}$ – mean pulmonary artery pressure; P_{LVED}, P_{RVED} – left and right end-diastolic pressure; SVR, PVR – systemic and pulmonary vascular resistance.

Table 7: Clinical scenarios simulated on the mock circulation loop (MCL) detailing the physiological scenario, modified MCL parameters, values, and literature supporting the values.

SVR - systemic vascular resistance; PVR - pulmonary vascular resistance; HR -heart rate.

Table 8: Steady-state haemodynamics for each controller during the simulated conditions. Green cells are values within the sweet spot limits while red cells fall outside the sweet spot limits.

ASLC- adaptive Starling-like control; SLC – Starling-like control; CSC– constant speed; HF - heart failure condition; RC – restored haemodynamic condition; CO ($\overline{Q_S}$ and $\overline{Q_P}$) – matched systemic and pulmonary flows; $\overline{P_{AO}}$ – mean aortic pressure; $\overline{P_{PA}}$ – mean pulmonary artery pressure; P_{LVED}, P_{RVED} – left and right end-diastolic pressure; $\overline{Q_{AV}}$, $\overline{Q_{PV}}$ – mean aortic and pulmonary valve flow; ω_{LVAD}, ω_{RVAD} – left and right ventricular assist device speed.